Nanoscale

Accepted Manuscript

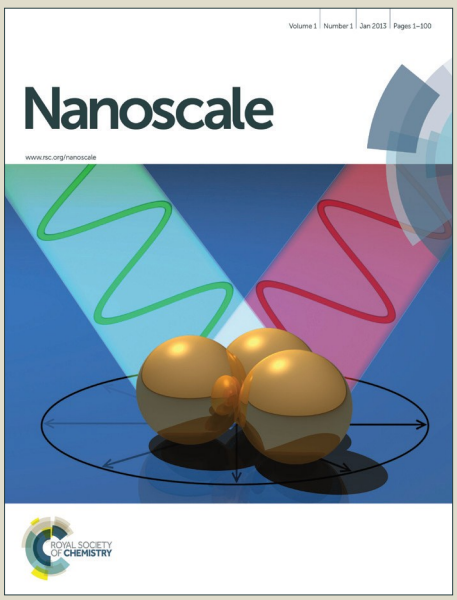

ROYAL SOCIETY OF CHEMISTRY

www.rsc.org/nanoscale

Arrays of High Quality SAM-Based Functions and their Application in Molecular Diode Based Logic

Albert Wan[1], *C. S. Suchand Sangeeth* [1], *Lejia Wang*[1], *Li Yuan*[1], *Li Jiang*[1], *and Christian A. Nijhuis*[1,2,3]*

[1]Department of Chemistry, National University of Singapore, 3 Science Drive, Singapore 117543

[2]Solar Energy Research Institute of Singapore (SERIS), 7 Engineering Drive 1, National University of Singapore, Singapore 117574, Singapore

[3]NUS Centre for Advanced 2D Materials and Graphene Centre, National University of Singapore, 2 Science Drive 3, Singapore 117542, Singapore.

Corresponding author:

E-mail: chmnca@nus.edu.sg

Abstract

This paper describes a method to fabricate a microfluidic top-electrode that can be utilized to generate arrays of self-assembled monolayer (SAM)-based junctions. The top-electrodes consist of a liquid-metal of GaO_x/EGaIn mechanically stabilized in microchannels and through-holes in polydimethylsiloxane (PDMS); these top-electrodes form molecular junctions by directly placing them onto the SAM supported by template-stripped (TS) Ag or Au bottom-electrodes. Unlike conventional techniques to form multiple junctions, our method does not require lithography to pattern the bottom-electrode and is compatible with TS bottom-electrodes, which are ultra-flat with large grains, free from potential contamination of photoresist residues, and do not have electrode-edges where the molecules are unable to pack well. We formed tunneling junctions with n-alkanethiolate SAMs in yields of ~80%, with good reproducibility and electrical stability. Temperature dependent *J*(V) measurements indicated that the mechanism of charge transport across the junction is coherent tunneling. To demonstrate the usefulness of these junctions, we formed molecular diodes based on SAMs with Fc head groups. These junctions rectify currents with rectification ratio *R* of 45. These molecular diodes were incorporated in simple electronic circuitry to demonstrate molecular diode-based Boolean logic.

Introduction

Molecular electronic devices based on self-assembled monolayers (SAMs) are useful for studying, and controlling, charge transport at the nano-scale.[1-5] The fabrication of reliable devices to generate molecular junctions with good reproducibility is still challenging, since it is difficult to form electrical contacts with molecules in a non-invasive manner and to minimize the number of defects in the junctions.[1,2,6-9] For practical purposes, it is important to demonstrate that the fabrication of the junctions can be scaled-up and that the junctions can be incorporated in electronic circuitry in a reproducible and reliable manner.[2,8,9] The challenge is to do so without compromising the quality of the junctions, i.e., to ensure the electronic properties of the junctions are determined by the molecules inside the junctions and not by defects or artifacts. Consequently, molecular junctions have rarely been incorporated in single electronic circuitry.[10-12] Here we describe the fabrication of arrays of junctions consisting of top-electrodes of GaO_x/EGaIn mechanically stabilized in a network of polydimethylsiloxane (PDMS) microchannels and through-holes, and SAMs supported by ultra-flat template-stripped (TS) bottom-electrodes that do not need to be patterned. This method forms junctions of good quality and reproducibility and produces molecular diodes with a rectification ratio $\langle \log_{10} R \rangle_G$ of 1.7 ± 0.8 ($R \equiv |J(-1.0\text{V})|/J(+1.0\text{V})$ where R is the rectification ratio, J is the current density, and the subscript G indicates that the log-average of R was obtained via a Gaussian fitting procedure (see below). These molecular diodes were used to demonstrate molecular diode-based Boolean logic.

Various methods that yield SAM-based junctions in large numbers have been reported before, but so far these methods did not yield junctions that rectified currents with large rectification ratios of >10.[13-18] We have demonstrated that GaO_x/EGaIn (eutectic mixture of 75.5% Ga and 24.5% In by weight with a highly conductive 0.7 nm thin layer of conductive GaO_x on the surface)[19] mechanically stabilized in a PDMS through-hole forms good electrical

contacts to SAMs by simply placing this top-electrode on the SAM.[22] We showed that defects in the electrode material,[20] subtle changes in the packing structure of the SAM,[5] or small amounts of impurities,[21] increase the leakage current across the junctions without affecting the yield of non-shorting junctions.[23,24] Currently it is not possible to determine the quality of the junctions directly, but good quality junctions should be dominated by the supramolecular structure of the junctions (and not by defects), and should have good electrical stabilities, high yields in working junctions with narrow distributions of the J(V) data (σ_{log}), i.e., high precision (See Supporting Information page S8-S9). Here σ_{log} is the log-standard deviation. Good quality junctions should also produce accurate data (See Supporting Information page S14-S15), i.e., data that are close to reference values. The reference values of the tunneling decay coefficient β, the pre-exponential factor J_0, and current density J for for GaO_x/EGaIn based junctions have been defined (see below),[22,25] and therefore, the accuracy can be determined. In addition, here we propose to use the rectification ratio as a qualitative indicator of junction quality. We have previously reported that the leakage current that flows across the molecular diode (in this work at positive bias) is highly sensitive to the supramolecular structure of the junctions [5, 21] and the presence of defects in the electrode materials[20] (the current that flows across the diodes at opposite bias is remarkably insensitive to defects). These observations imply that only junctions with well-defined supramolecular structures and low density of defects rectify with high values of R. In other words, junctions with high values of R are of good quality while junctions with low values of R are of low quality.

Here we describe a technique to fabricate a top-electrode that generates arrays of SAM-based junctions once it is in contact with the SAM. The top-electrodes can be directly placed onto the SAMs and re-used for 15-25 times. This method does not require patterning of the bottom-electrode and is compatible with ultra-flat and clean template-stripped electrodes

which are readily available in ordinary laboratory conditions.[26,27] This method forms junctions with high yields (~80%), with small distributions of the data (σ_{log} = 0.21), and with β (0.98 n^{-1}) and $\log_{10}|J_0|$ (2.34 A/cm^2) values that are very close to the reference values of GaO_x/EGaIn techniques which include cone-shaped GaO_x/EGaIn tips and GaO_x/EGaIn in PDMS channels.[22]**Error! Bookmark not defined.** In addition, we demonstrate that these arrays of junctions can be prepared with satisfactory quality and reproducibility in terms of precision and accuracy, between users and batches of top-electrodes. To demonstrate the usefulness of this method, we assembled Boolean logic gates based on molecular diodes.

Experimental

Preparation of the Ag^{TS} or Au^{TS} substrates. We prepared Ag^{TS} bottom-electrodes by following a procedure described in the literature.[26] A layer of 300 nm Ag (99.999%, Super Conductor Materials Inc, USA) was deposited on Si wafers (University wafers, USA) at a base pressure of ~2 $\times 10^{-6}$ mbar using a thermal evaporator (ShenYang KeYi, China). We deposited the first 50 nm of Ag at a rate of 0.5-0.7 Å and an additional 250 nm of Ag at a rate of ~1 Å. We glued clean glass slides (1 × 1 cm^2), which were rinsed with absolute ethanol and treated with a plasma of air for 5 minutes at 500 mTorr, to the Ag substrates using photo-curable optical adhesive (OA, Norland No. 61). The OA was cured for 1 hour using an ultraviolet light source (100 Watt) at a distance of ~0.5 m. We cut the Ag film around the glass slides using a razor blade and lifted the glass-OA-Ag stack off the Si-template using tweezers. The template-stripped surfaces were immersed in thiol-containing EtOH solution immediately. We prepared the Au^{TS} substrates by following a similar procedure as described above, but with thermally-cured epoxy (Epotex 353ND) cured at 80 ℃ for 8 hours. We have reported previously that the template-stripped metal surfaces using thermally cured epoxy as the glue yield surfaces of the same quality as those obtained with OA.[28]

Formation of n-alkanethiolate SAMs on Ag^{TS} substrates. We prepared $S(CH_2)_{n-1}CH_3$ (or in short SC_n; n is the number of carbons in the molecule**)** SAMs by following a well-known method.[22,23] We immersed the Ag^{TS} substrates in n-alkanethiol solutions (3 mM in absolute ethanol, AR grade, Merck), which were degassed by N_2 for 10 minutes prior to immersion. The n-alkanethiols (Sigma-Aldrich) were purified by recrystallization from absolute ethanol and stored at 4 ^oC prior to use. After 3 hours of SAM formation, we cleaned the substrates with copious amounts of absolute ethanol and blew the substrates to dryness in a stream of N_2.

Formation of $SCH_2PhCCPh(CH_2)_3Fc$ SAMs on Au^{TS} substrates. We prepared (1-(3-(3'-ferrocenylpropyl)diphenylacetylene))methanethiol ($HSCH_2PhCCPh(CH_2)_3Fc$) SAMs by following a previously reported procedure (See supporting information). The SAMs were prepared inside a glove box filled with argon (oxygen level of 0.1 ppm, water level of 1.0 ppm). We prepared 0.5 mM solution of $SCH_2PhCCPh(CH_2)_3Fc$ in absolute ethanol, and then immersed fresh template-stripped Au^{TS} into the solution. After the SAMs were formed over a period of time of 16 h at room temperature, we rinsed the substrates with dichloromethane (DCM) for around 5 seconds and copious amount of absolute ethanol, followed by drying in a stream of N_2.

Fabrication of the mold. We fabricated the molds using a two-step of photolithography process as described in detail in the Supporting Information and below.[22,29]

Preparation of PDMS with curing agent. We prepared the mixture of PDMS and its curing agent (Sylgard 184 Silicone Elastomer) following the procedure reported previously.[22] We mixed PDMS with its curing agent in a ratio of 10:1. After stirring the mixture of PDMS and the curing agent for around 1 minute, we placed it in a vacuum dessicator under a pressure of ~500 mTorr for 20 minutes to remove air bubbles.

Statistical analysis for data. We used previous reported methods to conduct the statistical analysis for the data in this work.[22,30] We formed junctions with different SC_n SAMs using three different top-electrodes on three different substrates. We collected *J*(V) curves from non-shorting junctions after the curves were stabilized, which normally occurred after 1-3 scan traces. We collected 20 traces and 20 retraces from each stabilized junction. After collecting the *J*(V) data, we plotted histograms of $\log_{10}|J|$ for each measured bias, and fitted Gaussians to the histograms to obtain the values of $<\log_{10}|J|>_G$ and their standard deviation (σ_{log}). Here we denote the values of $<\log_{10}|J|>_G$ for each type of SAM measured by three different top-electrodes as $<\log_{10}|J|>_{G,1}$, $<\log_{10}|J|>_{G,2}$, and $<\log_{10}|J|>_{G,3}$ and their standard deviations as $\sigma_{log,1}$, $\sigma_{log,2}$ and $\sigma_{log,3}$, and the value obtained from the total data collected by these electrodes as $<\log_{10}|J|>_{G,tot}$ and its standard deviation as $\sigma_{log,tot}$ (Tables 1 and S2; Figures S8-13). Based on eq 1, the $\log_{10}|J|$ values are expected to follow a normal distribution when the error of *d* follows a normal distribution.[22] We obtained the values of β and J_0 by plotting $<\log_{10}|J|>_{G,tot}$ versus carbon number (n_C) followed by fitting the data to eq 1 using a least-squares algorithm. In case of the *J*(V) measurements for $SCH_2PhCCPh(CH_2)_3Fc$ SAM junctions, we formed arrays of junctions using two different top-electrodes on two different substrates and collected *J*(V) curves for non-shorting junctions (Table S1). We obtained 600 *J*(V) curves in total and then analyzed the data by following the procedure reported previously.[5,22] The values of $\log|R|$ are considered to be normally distributed since $\log|J|$ follows a normal distribution. We calculated *R* values from all measured *J* values at -1.0 V and 1.0 V, and then plotted a histogram of all values of $\log_{10}|R|$, to which we fitted a Gaussian to determine the value of $<\log_{10}R>_G$ and its standard deviation.

Results and Discussion

Fabrication of the junctions

Figure 1 shows schematically the fabrication process of the microfluidic-based devices with the GaO_x/EGaIn mechanically stabilized in ten through-holes each of which insulated from the others. The PDMS was molded using masters that were obtained by a two-step lithography process on a Si/SiO_2 substrate (Figure S4) based on previously reported methods.[22,29] We fabricated two rows of five pillars (with a height of 60 μm and a diameter of 45 μm) each connected to a short line (line 1; 150 μm × 10 μm × 10 μm). The ends of lines 1 are connected to two long lines (line 2; 1.5 cm × 100 μm × 10 μm; Figure 1a). The inset of Figure 2a shows the scanning electron microscope (SEM) image of one of the pillars connected to line 1. We treated the mold with 1H,1H,2H,2H-perfluorooctyltrichlorosilane ($Cl_3Si(CH_2)_2(CF_2)_5CF_3$, FOTS) prior to use to minimize the interaction between the PDMS and the mold. After the treatment with FOTS, we spin-coated 20 μm of uncured PDMS (Sylgard 184) with curing agent (10:1) which fully covered the lines, but only partially covered the pillars on the mold (Figure 1b). After the PDMS layer was cured, we spin-coated an additional layer of 5 μm uncured PDMS with curing agent and aligned a cured PDMS block with ten channels (channel 3; 0.3 cm × 100 μm × 120 μm) that was prepared in a separate procedure using standard methods (see Supporting Information). The ends of channels 3 have punched holes which serve as in- and outlets to fill these channels with GaO_x/EGaIn. The channels were aligned to cover the pillars by using a stereomicroscope (Figure 1c) followed by curing the 5 μm thick PDMS layer. More uncured PDMS was added, and cured, to back fill the structures to improve the mechanical stability of PDMS slabs (Figure 1d). Finally, we peeled off the microfluidic chip from the mold and punched a hole at one of the ends of both channels 2 (Figure 1e).

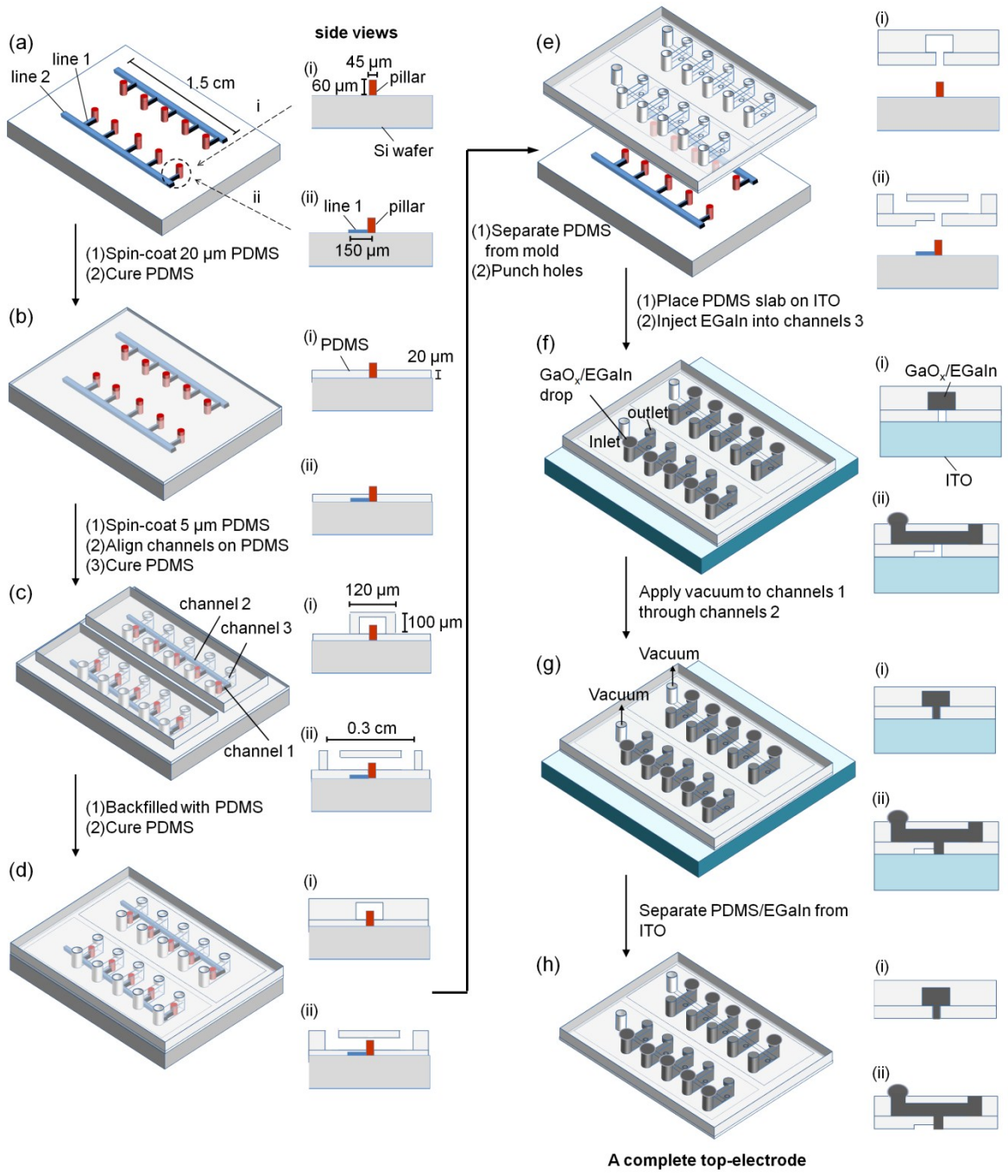

Figure 1. The fabrication process of the top-electrode. (a) The mold consists of two arrays of photoresist structures. Each array contains five pillars and five short lines (line 1) connected to a long line (line 2). (b) Spin-coating of a thin layer (20 μm) of PDMS which fully covered the lines, but partially covered the pillars. (c) Alignment of slabs of PDMS with channels 3 over the pillars. (d) Stabilization of PDMS structures by backfilling the voids with PDMS. (e) Separation of the PDMS microfluidic chip from the mold. (f) Injection of GaO_x/EGaIn into

channels 3 after the PDMS slab was placed on ITO. (g) Filling of the through-holes with GaO_x/EGaIn by applying vacuum to channel *via* channel 2 as indicated. (h) Separation of the top-electrode from ITO.

Figure 2a shows the optical image of the cross section of the PDMS chip with one of the through-holes connected to channel 1 linked with channel 2. To fill all channels 3 and the through-holes with GaO_x/EGaIn, we placed the PDMS chip on an ITO substrate to follow the GaO_x/EGaIn injection process by optical microscope. We filled the top channels one by one by placing drops of GaO_x/EGaIn at the inlets followed by applying vacuum (~500 mTorr) at the outlets of channels 3 (Figure 1f). Once all channels 3 were filled, we applied vacuum to the outlets of channels 2 (~500 mTorr) to fill five through-holes simultaneously *via* channels 1 and 2 (Figure 1g). The small diameters of channels 1 ensured that the GaO_x/EGaIn could not flow into these channels in the range of applied pressures because of the high surface tension of GaO_x/EGaIn (624 mN/m).[31,32]

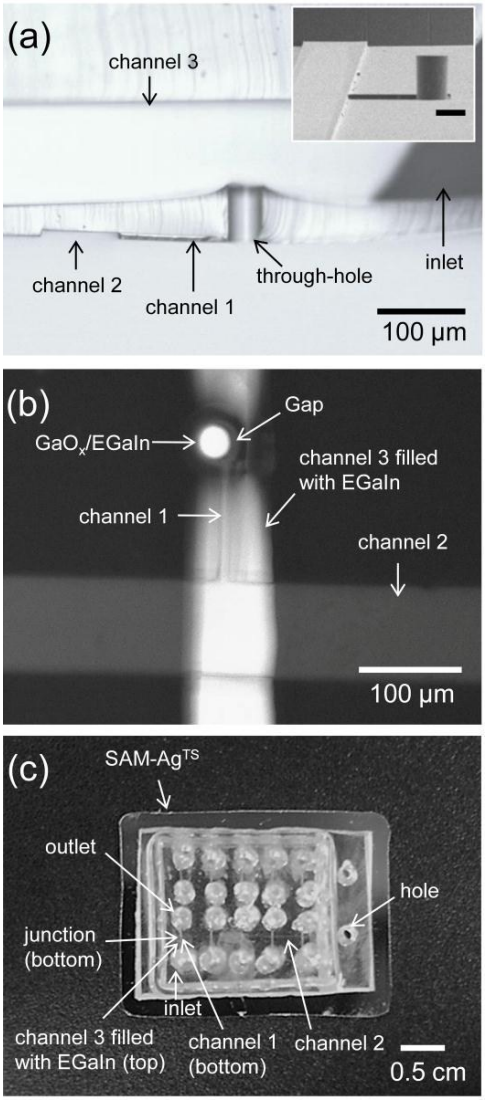

Figure 2. (a) An optical micrograph of a cross-section of a top-electrode showing the through-hole before it was filled with the liquid-metal. The inset shows a SEM image of one of the pillar-line structures of the mold. Scale bar: 50 µm. (b) Optical image (viewed through the ITO) of one of the though-holes filled with GaO_x/EGaIn. (c) Photograph of a complete device (top view).

The filling of GaO_x/EGaIn into the through-holes was verified optically and by simply measuring the resistance between the ITO substrate and the GaO_x/EGaIn at the inlet of channel 3 using a multi-meter. Figure 2b shows the optical image (obtained through the ITO) of one of the PDMS through-holes filled with GaO_x/EGaIn on an ITO substrate. The diameter

of the GaO_x/EGaIn was determined to be 35.2 ± 1.8 μm with a gap of 9.6 ± 1.0 μm between GaO_x/EGaIn and the side wall of the through-hole likely due to the surface tension of GaO_x/EGaIn. We separated the top-electrode from the ITO substrate (Figure 1h), and placed it on SAMs on Ag^{TS} or Au^{TS} to form arrays of junctions (Figure 3a). Figure 3c shows a schematic diagram of one junction within the device and a photograph of a complete device is given in Figure 2c.

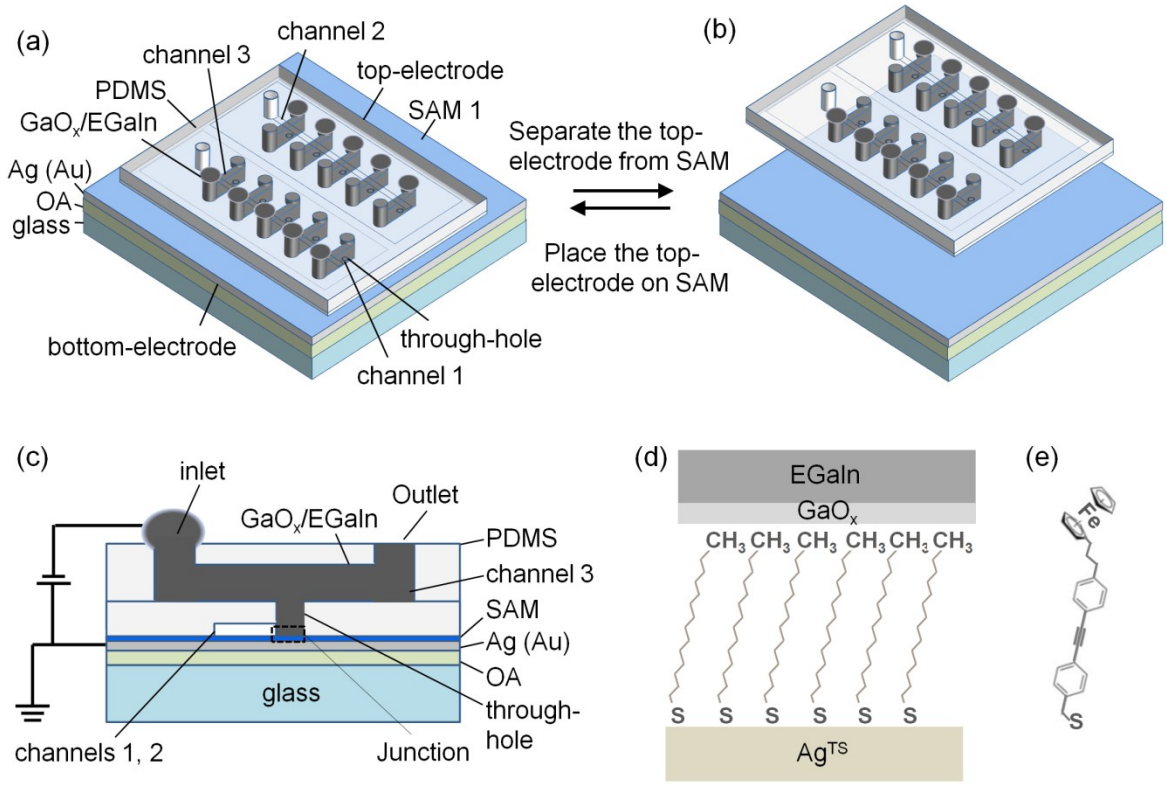

Figure 3. (a) and (b) Schematic illustrations (not drawn to scale) of the reversible placement of the top-electrode on the SAM. (c) Side view of one of the junctions. (d) Schematic diagram of the junction (not drawn to scale) with a SAM of $S(CH_2)_{13}CH_3$. (e) The molecular structure of $SCH_2PhCCPh(CH_2)_3Fc$.

Electrical characterization of the junctions

To study the electrical characteristics of the SAM-based junctions, we prepared three top-electrodes each of which was placed in contact with five different SC_n SAMs with n = 10, 12, 14, 16 and 18, on Ag^{TS} substrates. Thus we obtained three data-sets of 50 junctions (10 junctions for each value of n) per top-electrode (Table 1). Figure S7a shows a typical AFM image of an Ag^{TS} surface, which has a root mean square (rms) roughness of 0.6 nm over an area of $1 \times 1\ \mu m^2$. The top-electrodes were placed on the SAMs and formed good electrical contact with the SAM-Ag^{TS} most of the times (Figure 3a). Applying vacuum to channels 2 restored good electrical contacts with the SAM when needed. To form a complete circuit, a tungsten probe mounted on a micromanipulator was contacted with the GaO_x/EGaIn drop at the inlet of the top-electrode, while another probe was placed on the substrate (Figure 3c). We measured 20 J(V) traces over the range of biases of -0.50 to 0.50 V (one trace ≡ 0 V → 0.50 V → -0.50 V → 0V) at intervals of 25 mV. New junctions were formed by removing the top-electrode from the substrate and placing it on a new substrate with a different type of SAM (Figures 3a and b).

Table 1. The total number of non-shorting data (N_J), the yields of working devices, the values of β, $\langle\log|J_0|\rangle_G$ and σ_{log} at -0.50 V of J(V) measurements for n-alkanethiolate-based junctions.

top-electrode	junctions	non-shorting junctions	yield (%)[a]	N[b]	β (n_C^{-1})	$\langle\log_{10}\|J_0\|\rangle_G$	σ_{log}
top-electrode 1	50	40	80	1600	0.94 ± 0.02	2.04	0.15[c]
top-electrode 2	50	39	78	1560	0.98 ± 0.02	2.29	0.17[c]
top-electrode 3	50	41	82	1640	1.00 ± 0.07	2.46	0.16[c]
all	150	120	80	4800	0.98 ± 0.02	2.34	0.16
reference [22]	-	-	-	-	1.00 ± 0.02	2.38 – 3.40	-

[a]The yield of non-shorting junctions. [b]The number of total scan traces (including trace and retrace). [c]The average value of each standard deviation (values of $\sigma_{log,1}$, $\sigma_{log,2}$, and $\sigma_{log,3}$ in Table S2) of $\langle\log_{10}|J|\rangle_G$ obtained for junctions incorporated with 1-decanethiolate [$S(CH_2)_9CH_3$], 1-dodecanethiolate [$S(CH_2)_{11}CH_3$], 1-tetradecanethiol [$S(CH_2)_{13}CH_3$], 1-hexadecanethiol [$S(CH_2)_{15}CH_3$] and 1-octadecanethiol [$S(CH_2)_{17}CH_3$] SAMs.

We recorded statistically large data set (4800 J(V) curves in total) and the yields of non-shorting junctions were 78-82% (Table 1), which is similar to other techniques based on GaO_x/EGaIn top electrodes.[22,25,33-34] By fitting the histograms of all values of $\log_{10}|J|$ for a given applied bias to Gaussians, the average values of J ($<\log_{10}|J|>_{G,tot}$) and their standard deviation ($\sigma_{log,tot}$) were determined. This procedure was repeated for each measured bias to construct the log-average J(V) curves shown in Figure 4a. Figure S8 shows the histograms of all $\log_{10}|J|$ values at -0.50 V and +0.50 V, and Table S2 shows the values of $<\log_{10}|J|>_G$ and σ_{log} for the junctions obtained using each of the three top-electrodes for each type of junction. Although the aim of this work is to report a method to fabricate arrays of junctions that is compatible with readily available TS surfaces,[26] this platform can also be extended to patterned TS bottom-electrodes to yield devices with arrays of junctions of which both the top- and bottom-electrodes can be individually addressed (See Supporting Information pages S22-S23).

We found that the values of $<\log_{10}|J|>_{G,total}$ are close to reference values determined for other variations of the GaO_x/EGaIn technique (Table S2) which are given in references 22 and 25. The values of $\sigma_{log,1}$, $\sigma_{log,2}$ and $\sigma_{log,3}$, obtained by measuring each SAM using three different top-electrodes, range from 0.07 to 0.27 for each array of 10 junctions (Table S2) and their average values range from 0.15 to 0.17 for each top-electrode (Table 1). Combining all data to determine $<\log_{10}|J|>_{G,tot}$ resulted in a small increase of $\sigma_{log,tot}$ to 0.21 (Table 1). From these observations, we conclude that the variation from electrode-to-electrode is small and the data are precise and accurate.

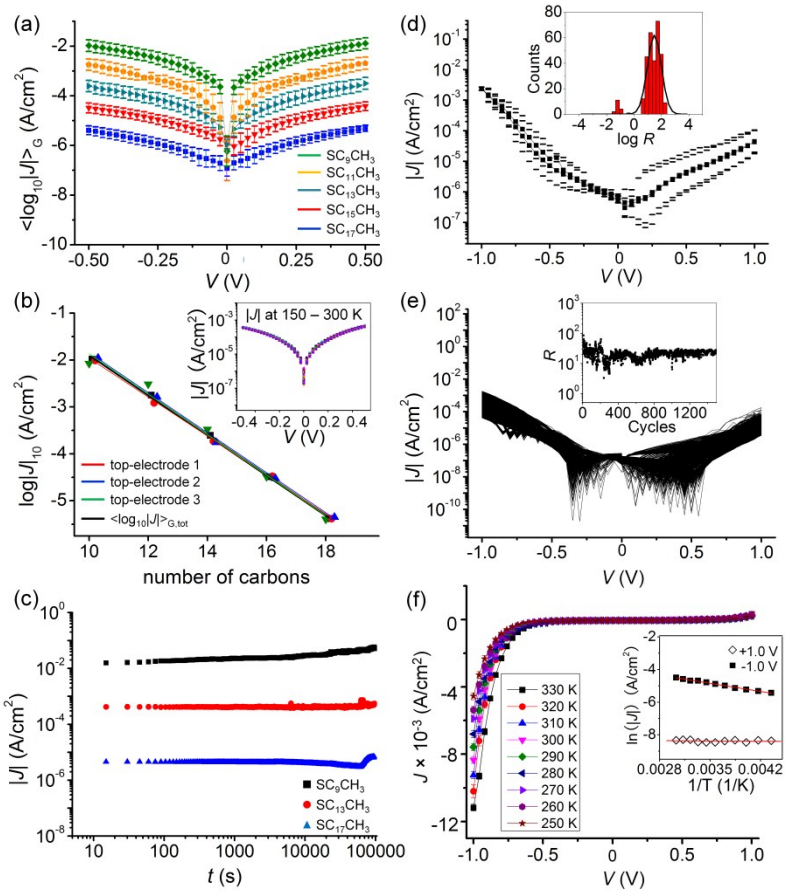

Figure 4. (a) Plots of $\langle \log_{10}|J| \rangle_{G,tot}$ vs. applied bias for junctions with $SC_{n-1}CH_3$ SAMs with n = 10, 12, 14, 16, and 18. The error bars represent σ_{log} values. (b) Plots of $\langle \log_{10}|J| \rangle_{G,1}$, $\langle \log_{10}|J| \rangle_{G,2}$ and $\langle \log_{10}|J| \rangle_{G,3}$ at -0.50 V versus chain length. Solid lines are fits to eq 1. The inset shows the J(V) curves of a $S(CH_2)_{14}CH_3$ junction recorded in steps of 10 K over the range of temperatures of 150 to 300 K. (c) Retention characteristics at constant bias at -0.50 V for 100 000 seconds. Data were collected at intervals of 15 seconds. (d) The log-average J(V) curves of junctions with $SCH_2PhCCPh(CH_2)_3Fc$ SAMs. The inset shows the histogram of R with a Gaussian fit to this histogram. (e) 1500 J(V) curves for junctions with a $SCH_2PhCCPh(CH_2)_3Fc$ SAM measured by continuous sweeping the bias between -1.0 and 1.0 V (four seconds per cycle). The inset shows the value of R plotted against the bias cycle number. (f) The J(V) curves of the $SCH_2PhCCPh(CH_2)_3Fc$ junction measured at different

temperatures (T = 250 – 330 K). The inset shows the Arrhenius plots for values of $|J|$ measured at +1.0 and -1.0 V.

The mechanism of charge transport across SC_n SAM-based junctions has been studied across different test-beds and is believed to be coherent tunneling,[13,22,25,33] where the value of J at a given voltage decreases exponentially with the thickness of the SAMs (d) given by eq. 1 where β is the tunneling decay constant, d_{SAM} is the thickness of the SAM, and J_0 is the pre-exponential factor.**Error! Bookmark not defined.**,[25] To determine the mechanism of charge transport across our junctions, we studied their electrical characteristics as a function of n_c and temperature.

$$J = J_0 e^{-\beta d_{SAM}} \quad (1)$$

Figure 4b shows three plots of $\langle \log_{10}|J| \rangle_{G,1}$, $\langle \log_{10}|J| \rangle_{G,2}$ or $\langle \log_{10}|J| \rangle_{G,3}$ versus n_C obtained by using three different top-electrodes and the plot of $\langle \log_{10}|J| \rangle_{G,tot}$ using all data versus n_C. The values of J decay exponentially as a function of n_C as expected from eq. 1. The β values were in the range of 0.94-1.00 n_C^{-1} (0.75-0.80 Å^{-1}; Table 1), which agree well with the consensus value (0.80 Å^{-1}; 1.0 n_C^{-1}) measured across different test-beds reported in the literature.[1,33] The $\log_{10}J_0$ values range from 2.0-2.5 A/cm^2, which are very close to the reference values determined by averaging all reported values measured by using other types of GaO_x/EGaIn-based techniques.[22]

Temperature-dependent measurements provide information of the mechanism of charge-transport across the junction. We varied the temperature in the range of 150-300 K of a device incorporating a $S(CH_2)_{13}CH_3$ SAM in a probe station at the pressure of 1 $\times 10^{-5}$ bar. We found that the electrical characteristics of the junctions were not measurably altered by lowering the pressure or changing the temperature (inset of Figure 4b). The device shorted below 150 K likely because of the differences in the thermal expansion coefficients of the

different components of the junctions.[22,35] The temperature-independency of the *J*(V) characteristic indicates that the mechanism of charge transport across the junction is coherent tunneling in agreement with data reported for other types of SAM-based junctions with SC_n SAMs.[22,33,34]

Electrical stability

The electrical stability of the junctions was examined by continuous voltage cycling and bias stressing. Figure 4c shows the retention characteristics of the devices under a bias stress of -0.50 V for 10^5 seconds. Figure S14 shows that the devices were electrically stable for 1500 cycles of voltages (one cycle ≡ 0 V → 0.50 V → -0.50 V → 0V). From these experiments we conclude that the junctions were stable and did not short before we stopped the measurements.

Molecular diodes

Junctions with SAMs with Fc termini of the form SC_nFc rectify currents in different types of junctions.[5,20,21,35-37] We first collected 600 *J*(V) curves in total for $SCH_2PhCCPh(CH_2)_3Fc$ SAM junctions in 75% yield (Table S1), and then fitted to the histogram of *R* a Gaussian to determine the value of $\langle \log_{10}R \rangle_G$ (see Supporting Information pages S5-S7 for details of the SAM characterization). We modified the surface of the PDMS of the top-electrode with 3-(aminopropyl)triethoxysilane (APTES) prior to the injection of GaO_x/EGaIn to reduce the adhesion between the top-electrode and the SAM (see Supporting Information). Thus, neither the SAMs nor the GaO_x/EGaIn surfaces were exposed to APTES. Figure 4d shows the log-average *J*(V) curves of the junctions incorporating SAMs of $SCH_2PhCCPh(CH_2)_3Fc$. These junctions are good molecular diodes: the junctions conduct at negative bias (forward bias), but block the current at positive bias (reverse bias) with

$\langle \log_{10} R \rangle_G = 1.7 \pm 0.8$ (inset of Figure 4d). Figure 4e shows that that the *J*(V) curves and the values of *R* did not change significantly by continuous sweeping the bias between -1.0 to 1.0 V (trace and re-trace) for 1500 times. We note that the "spikes" in the low bias regime are caused by a small current that flows at zero bias which appear as anomalies in the semi-log plot (see reference 12 for details) and are not caused by the GaO_x layer (see reference 19).

To determine the mechanism of charge transport across this diode, we performed *J*(V,T) measurements over the range of temperatures of 250 – 330 K (Figure 4f). The inset of Figure 4f also shows the Arrhenius plots at both -1.0 and +1.0 V. The results show that the diode changes the mechanism of charge transport from direct tunneling at positive bias to sequential tunneling at negative bias. This bias induced change in the mechanism of charge transport is similar to that observed for junctions with $SC_{11}Fc$ SAMs on Ag^{TS} bottom-electrodes with GaO_x/EGaIn top-electrodes[5,24] (and has been confirmed by others[38-40]). Therefore we believe that here the same mechanism of charge transport applies. The highest occupied molecular orbital (HOMO) of the $SCH_2PhCCPh(CH_2)_3Fc$ is located at the Fc units (the three CH_2 units are long enough to energetically decouple the Fc unit and diphenylacetylene group) and is -5.0 eV in energy with respect to vacuum.[28] The diphenylacetylene (PhCCPh) group has a large energy gap (4.4 to 4.9 eV)[41] and thus we do not believe that the energy levels associated with the backbone of the molecule participate in the mechanism of charge transport measurements considering our small bias window of ±1.0 V. The Fermi-level of the GaO_x/EGaIn electrode is -4.2 eV,[42] and that of the Au^{TS} electrode with a SAM is -4.3 eV.[42,43] The HOMO follows the Fermi-level of the top-electrode and can fall in the energy window defined by the Fermi-levels of the electrodes at sufficiently large bias and participates in the mechanism of charge transport resulting in indirect tunneling. In contrast, at positive bias the HOMO cannot fall in the energy window defined by the Fermi-levels of the electrodes in the applied bias range resulting in direct tunneling. From the

Arrhenius plots we determined an activation energy E_a of 72 ± 5 meV by fitting the data at -1.0 V to the Arrhenius equation (eq 2) (the error indicates the 95% confidence level of the fit) where k_B is the Boltzmann constant.[34]

$$J = J_0 \exp(-E_a / k_B T) \quad (2)$$

The activation energy is close to the value reported for $S(CH_2)_{11}Fc$ SAM-based junctions and is associated with the reorganization energy that is required for the Fc units to accommodate a positive charge.[34]

Molecular-diode logic gates. A logic gate performs a logic operation based on the Boolean function with one or more inputs and generates a single output, and can be generated by utilizing diodes or transistors.[44-46] By using devices with arrays of $SCH_2PhCCPh(CH_2)_3Fc$ SAM junctions (Figure 3e), we were able to configure two-input OR and AND logic gates using two molecular diodes as shown in the insets of Figure 5. Here we used DC voltages as inputs and measured the output as voltage across a 10 MΩ resistor. We applied 0 and -1 V as the low and high input voltages to the diodes and the output of the logic gate was measured as the voltage drop across the resistor. Figure 5a shows the truth table of the OR gate measured experimentally and the truth table agrees well with the characteristic of an OR gate, in which the output is high when any of the input is set to be high. The OR gate showed a low output (logic 0) when both input voltages were low (0 V) and a high output (logic 1) when either or both of the input voltages were high (-1 V). When one of the inputs was high, one of the diodes conducted and developed a voltage drop across the constant resistor. When both inputs were set to be high, both diodes were forward biased and allowed current to pass through the junctions. Since the diodes were connected in parallel, the output voltage with two high inputs was the same as the one with only one high input voltage (logic 1).The difference between the high and low state voltages was found to be around two orders of magnitude reflecting the high values of R of these two diodes of 95 and 1.0×10^2. In the case of the

AND gate, we observed a low output (logic 0) when either one or both of the inputs were low (0 V) as indicated in the truth table (Figure 5b). When both inputs were high (-1 V), both diodes were reverse-biased with resistances larger than the constant resistor, causing a small voltage drop across the resistor and hence a high output voltage was observed (logic 1).

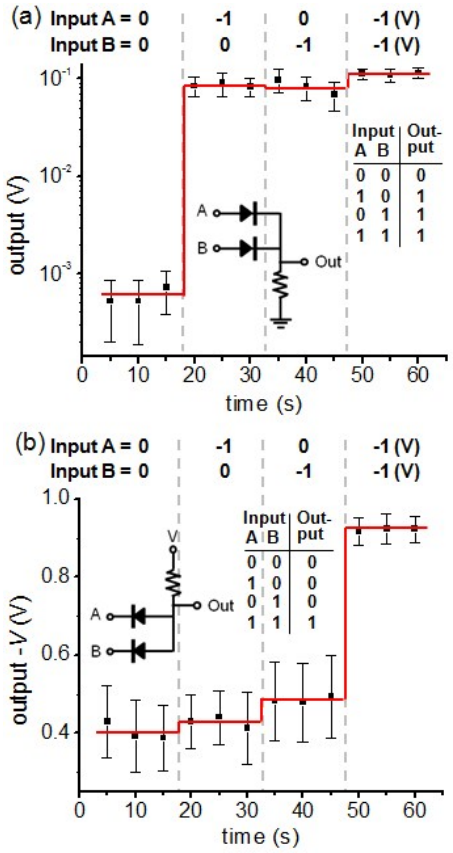

Figure 5. Schematic drawing of the electronic circuits and the experimentally measured truth tables for (a) OR and (b) AND logic gates formed by arrays of junctions with molecular diodes incorporated in the device. The inputs (A and B) are indicated at the top of the graphs. The red line is a guide to the eye for the measured output voltage. Insets show the configurations of the circuits and the measured truth tables.

Conclusions

Here we report a new technique to fabricate arrays of SAM-based tunnel junctions. The top-electrode consisted of the non-Newtonian liquid-metal of GaO_x/EGaIn mechanically stabilized in arrays of ten individual micrometer sized through-holes in PDMS; these top-electrodes formed highly reproducible electrical contacts to SAMs. Moreover, the top-electrode is compatible with SAMs formed on ultra-flat template-stripped bottom electrodes. The electrodes do not need to be patterned and are free from photoresist residues, and electrode-edges where SAM cannot pack well. We showed that statistically large numbers of J(V) data (N = 1600) can be obtained using a single chip with an array of ten junctions. The electrical characteristics of n-alkanethiolate junctions between different junctions within the same device and between different top-electrodes were found to have a small variation (average values of $\sigma_{\log,1}$ = 0.15, $\sigma_{\log,2}$ = 0.17, $\sigma_{\log,3}$ = 0.16 and $\sigma_{\log,tot}$ = 0.21), which indicates that the electrical measurements using this method are precise. The values of $<\log_{10}|J|>_G$, β, and J_0 are all close to the reference values (Tables 1 and S1), revealing that our measurements are accurate. Moreover, the junctions within the device have good stability under continued voltage cycling (>1500 cycles) and bias stressing (up to 1.0×10^5 s). Therefore, we conclude that the arrays of SAM-based junctions are of good quality because of the large yield (80%) in working junctions, high reproducibility in terms of precision and accuracy, high stability against electrical biasing, and high values or R. Although we formed ten individual junctions in a single device in this work, in principle larger number of junctions can be generated using the same fabricating method. Furthermore, we have demonstrated that this technique is useful to form arrays of molecular diodes to construct molecular diode-based Boolean logic gates. Although this method generates junctions without electrode edges, the electrode material itself still contains grain boundaries at which SAMs cannot pack well. We are currently developing methods to reduce the number of grain boundaries inside the junctions.

Acknowledgements

The authors gratefully thank the Singapore National Research Foundation (NRF) for financial support under CRP award No. NRF-CRP8-2011-07 and NUS Centre for Advanced 2D Materials and Graphene Centre for supporting this research.

References

[1] H. B. Akkerman and B. de Boer, *J. Phys.:Condens. Mat.*, 2008, **20**, 013001.
[2] H. Song, M. A. Reed and T. Lee, *Adv. Mater.*, 2011, **23**, 1583-1608.
[3] J. Y. Song and H. Song, *Curr. Appl. Phys.*, 2013, **13**, 1157-1171.
[4] S. F. Tan, L. Wu, J. K.W. Yang, P. Bai, M. Bosman and C. A. Nijhuis, *Science*, 2014, **343**, 1496-1499.
[5] N. Nerngchamnong, L. Yuan, D. C. Qi, J. Li, D. Thompson and C. A. Nijhuis, *Nat. Nanotechnol.*, 2013, **8**, 113-118.
[6] G. Wang, T. W. Kim and T. Lee, *J. Mater. Chem.*, 2011, **21**, 18117-18136.
[7] H. Haick and D. Cahen, *Prog. Surf. Sci.*, 2008, **83**, 217-261.
[8] R. L. McCreery and A. J. Bergren, *Adv. Mater.*, 2009, **21**, 4303-4322.
[9] X. Yu, R. Lovrinčić, O. Kraynis, G. Man, T. Ely, A. Zohar, T. Toledano, D. Cohen and A. Vilan, *Small*, 2004, **24**, 5151-5160.
[10] H. B. Akkerman, P. W. M. Blom, D. M. de Leeuw and B. de Boer, *Nature*, 2006, **441** 69-72.
[11] R. McCreery, A. Bergren, A. Morteza-Najarian, S. Y. Sayed and H. Yan, *Farad. Discuss.*, 2014, **172**, 9-25.
[12] C. A. Nijhuis, W. F. Reus, A. C. Siegel and G. M. Whitesides, *J. Am. Chem. Soc.*, 2011, **113**, 15397-15411.
[13] M. L. Chabinyc, X. Chen, R. E. Holmlin, H. Jacobs, H. Skulason, C. D. Frisbie, V. Mujica, M. A. Ratner, M. A. Rampi and G. M. Whitesides, *J. Am. Chem. Soc.*, 2002, **124**, 11730-11736.
[14] M.-K. Ng, D.-C. Lee and L. Yu, *J. Am. Chem. Soc.*, 2002, **124**, 11862-11863.
[15] X. Chen, Y.-M. Jeon, J.-W. Jang, L. Qin, F. Huo, W. Wei and C. A. Mirkin, *J. Am. Chem. Soc.*, 2008, **130**, 8166-8168.
[16] S. Lenfant, C. Krzeminski, C. Delerue, G. Allan and D. Vuillaume, *Nano Lett.*, 2003, **3**, 741-746.
[17] A. Aviram and M. A. Ratner, *Chem. Phys. Lett.*, 1974, **29**, 277-283.
[18] R. Stadler, V. Geskin and J. Cornil, *J. Phys:Condens. Matter.*, 2008, **20**, 374105.
[19] C. S. Suchand Sangeeth, A. Wan and C. A. Nijhuis, *J. Am. Chem. Soc.*, 2014, **136**, 11134-11144.
[20] L. Yuan, L. Jiang, D. Thompson and C. A. Nijhuis, *J. Am. Chem. Soc.*, 2014, **136**, 6554-6557.
[21] L. Jiang, L. Yuan, L. Cao and C. A. Nijhuis, *J. Am. Chem. Soc.*, 2014, **136**, 1982-1991.
[22] A. Wan, L. Jiang, C. S. Suchand Sangeeth and C. A. Nijhuis, *Adv. Func. Mater.*, 2014, **24**, 4442-4456.

[23] L. Yuan, L. Jiang, B. Zhang and C. A. Nijhuis, *Angew. Chem. Int. Ed.*, 2014, **53**, 3377-3381.
[24] L. Jiang, C. S. Suchand Sangeeth, A. Wan, A. Vilan and C. A. Nijhuis, *J. Phys. Chem. C*, 2015, **119**, 960-969.
[25] F. C. Simeone, H. J. Yoon, M. M. Thuo, J. R. Barber, B. Smith and G. M. Whitesides, *J. Am. Chem. Soc.* 2013, **135**, 18131-18144.
[26] E. A. Weiss, G. K. Kaufman, J. K. Kriebel, Z. F. Li, R. Schalek and G. M. Whitesides, *Langmuir*, 2007, **23**, 9686-9694.
[27] L. Jiang, T. Wang and C. A. Nijhuis, *Thin Solid Films*, 2015, **593**, 26-39.
[28] L. Yuan, R. Breuer, L. Jiang, M. Schmittel and C. A. Nijhuis, *Nano Lett*. 2015, **15**, 5506-5512.
[29] E. P. Kartalov, C. Walker, C. R. Taylor, W. F. Anderson and A. Scherer, *P. Natl. Acad. Sci.USA*, 2006, **103**, 12280-12284.
[30] W. F. Reus, C. A. Nijhuis, J. R. Barber, M. M. Thuo, S. Tricard and G. M. Whitesides, *J. Phys. Chem. C*, 2012, **116**, 6714-6733.
[31] G. J. Hayes, J. H. So, A. Qusba, M. D. Dickey and G. Lazzi, *IEEE T., Antenn. Propag.*, 2012, **60**, 2151-2156.
[32] M. D. Dickey, R. C. Chiechi, R. J. Larsen, E. A. Weiss, D. A. Weitz and G. M. Whitesides *Adv. Funct. Mater.*, 2008, **18**, 1097-1104.
[33] C. A. Nijhuis, W. F. Reus, J. R. Barber and G. M. Whitesides, *J. Phys. Chem. C*, 2012, **116**, 14139-14150.
[34] C. A. Nijhuis, W. F. Reus, J. R. Barber, M. D. Dickey and G. M. Whitesides, *Nano Lett.*, 2010, **10**, 3611-3619.
[35] H. Jeong, D. Kim, G. Wang, S. Park, H. Lee, K. Cho, W.-T. Hwang, M.-H. Yoon, Y. H. Jang, H. Song, D. Xiang and T. Lee, *Adv. Func. Mater*., 2014, **24**, 2472-2480.
[36] L. Müller-Meskamp, S. Karthäuser, H. J. V. Zandvilet, M. Homberger, U. Simon and R. Waser, *Small*, 2009, **5**, 496-502.
[37] E. D. Mentovich, N. R.-S. Kalifa, M. Gozin, V. Mujica, T. Hansen and S. Richter, *J. Phys. Chem. C*, 2013, **117**, 8468-8474.
[38] H. Jeong, D. Kim, G. Wang, S. Park, H. Lee, K. Cho, W.-T. Hwang, M.-H. Yoon, Y. H. Jang, H. Song, D. Xiang, T. Lee, *Adv. Funct. Mater*. 2014, **24**, 2472.
[39] E. D. Mentovich, N. Rosenberg-Shraga, I. Kalifa, M. Gozin, V. Mujica, T. Hansen, S. Richter, *J. Phys. Chem. C* 2013, **117**, 8468.
[40] L. Müller-Meskamp, S. Karthäuser, H. J. W. Zandvliet, M. Homberger, U. Simon and R. Waser, *Small* 2009, **5**, 496-502.
[41] Y. Li, J. Zhao, Y. Yin, H. Liu and G. Yin, *Phys. Chem. Chem. Phys*., 2007, **9**, 1186.
[42] K. S. Wimbush, R. M. Fratila, D. D. Wang, D. C. Qi, C. Liang, L. Yuan, N. Yakolev, K. P. Loh, D. N. Reinhoudt and A. H. Velders, *Nanoscale*, 2014, **6**, 11246-11258.
[43] Y. P. Liu, L. Yuan, M. Yang, Y. Zheng, L. J. Li, L. B. Gao, N. Nernchamnong, C. T. Nai, C. S. Suchand Sangeeth, Y. P. Feng, C. A. Nijhuis and K. P. Loh, *Nat. Commun*., 2014, **5**, 5461.
[44] T. L. Floyd, 1997 Digital Fundamentals; Prentice-Hall International Inc.: Upper Saddle River, NJ.
[45] Y. Huang, X. F. Duan, Y. Cui, L. J. Louhon, K. H. Kim and C. M. Lieber, *Science*, 2001, **294**, 1313-1317.
[46] G. de Ruiter and M. E. van der Boom, *Acc. Chem. Res*., 2011, **44**, 563-573.